Observation of collective coupling between an engineered ensemble of macroscopic artificial atoms and a superconducting resonator

Kosuke Kakuyanagi,[1,*] Yuichiro Matsuzaki,[1] Corentin Déprez,[1] Hiraku Toida,[1]
Kouichi Semba,[2] Hiroshi Yamaguchi,[1] William J. Munro,[1] and Shiro Saito[1]

[1] *NTT Basic Research Laboratories, NTT Corporation, 3-1 Morinosato-Wakamiya, Atsugi, Kanagawa, 243-0198, Japan.*
[2] *National Institute of Information and Communications Technology, 4-2-1, Nukuikitamachi, Koganei-city, Tokyo 184-8795 Japan*

(Dated: June 15, 2016)

The hybridization of distinct quantum systems is now seen as an effective way to engineer the properties of an entire system leading to applications in quantum metamaterials, quantum simulation, and quantum metrology. One well known example is superconducting circuits coupled to ensembles of microscopic natural atoms. In such cases, the properties of the individual atom are intrinsic, and so are unchangeable. However, current technology allows us to fabricate large ensembles of macroscopic artificial atoms such as superconducting flux qubits, where we can really tailor and control the properties of individual qubits. Here, we demonstrate coherent coupling between a microwave resonator and several thousand superconducting flux qubits, where we observe a large dispersive frequency shift in the spectrum of 250 MHz induced by collective behavior. These results represent the largest number of coupled superconducting qubits realized so far. Our approach shows that it is now possible to engineer the properties of the ensemble, opening up the way for the controlled exploration of the quantum many-body system.

arXiv:1606.04222v1 [quant-ph] 14 Jun 2016

Quantum science and technology have reached a very interesting stage in their development where we are now beginning to engineer the properties that we require of our quantum systems [1, 2]. Hybridization is a core technique in achieving this. An additional (or ancilla) system can be used to greatly change not only the properties of the overall system, but also its environment [3–5].

Specifically, a hybrid system composed of many qubits and a common field such as cavity quantum electrodynamics [6, 7] may provide an excellent way of realizing such quantum engineering, leading to an interesting investigation of many-body phenomena including quantum simulations [8, 9], superradiant phase transitions [10–15], spin squeezing [16–18], and quantum metamaterials [19–25]. In this regard, one of the ways to realize such a system is to employ superconducting circuits coupled to electron spin ensembles where basic quantum control such as memory operations have been demonstrated [26–30]. If we are to investigate quantum many-body phenomena, we will need control over the ensemble. In most typical superconducting circuit-ensemble hybrid experiments, the ensemble has been formed from a collection of either atoms or molecules with examples including nitrogen vacancy centers [26–28, 31], ferromagnetic magnons [32], and bismuth donor spins in silicon [33]. In these cases, the properties of the atomic ensemble system are basically defined as the ensemble is formed, and are difficult to change. However, our ensembles could be composed of artificial atoms such as superconducting qubits.

Superconducting qubits are macroscopic two-level systems with a significant degree of design freedom [34, 35]. Josephson junctions provide the superconducting circuit with non-linearity, and we can tailor the qubit properties by changing the design of the circuit. Moreover, in contrast to natural atoms that are the size of angstrom, the size of the superconducting circuit is around $1-10$ μm and so we can change the properties of individual qubit with a time scale of nano-seconds by using a control line coupled to each qubit. Actually, frequency tunability [36, 37], coherence time control [38], tunable coupling strength [39], engineering selection rules of qubit transitions [40], and control of the level structure of the qubit [41], have been demonstrated with the superconducting qubits. These show the feasibility to engineer the properties of the superconducting circuit.

Besides the tunability, another key issue in terms of observing interesting quantum phenomena is how to scale the number of the qubits. Collective coupling between three superconducting transmon qubits and a cavity field has been demonstrated [42], and a multi partite entanglement has been generated with this system [43]. Quantum critical behavior has been experimentally investigated with a system where four superconducting phase qubits are coupled with a resonator [44]. Also, there has been an experimental demonstration in which 20 superconducting qubits are fabricated and 8 qubits show a collective coupling [45]. However, the number of coherently coupled superconducting qubits in the previously reported demonstration may not be large enough for practical applications, and so we need to extend the system to more qubits.

Here, we perform an experiment where thousands of superconducting flux qubits are coupled with a superconducting resonator. Since the resonant frequency of the superconducting flux qubits is sensitive to small changes in the fabrication conditions [46], the superconducting flux qubits suffer from inhomogeneous broadening. However, the collective coupling of superconduct-

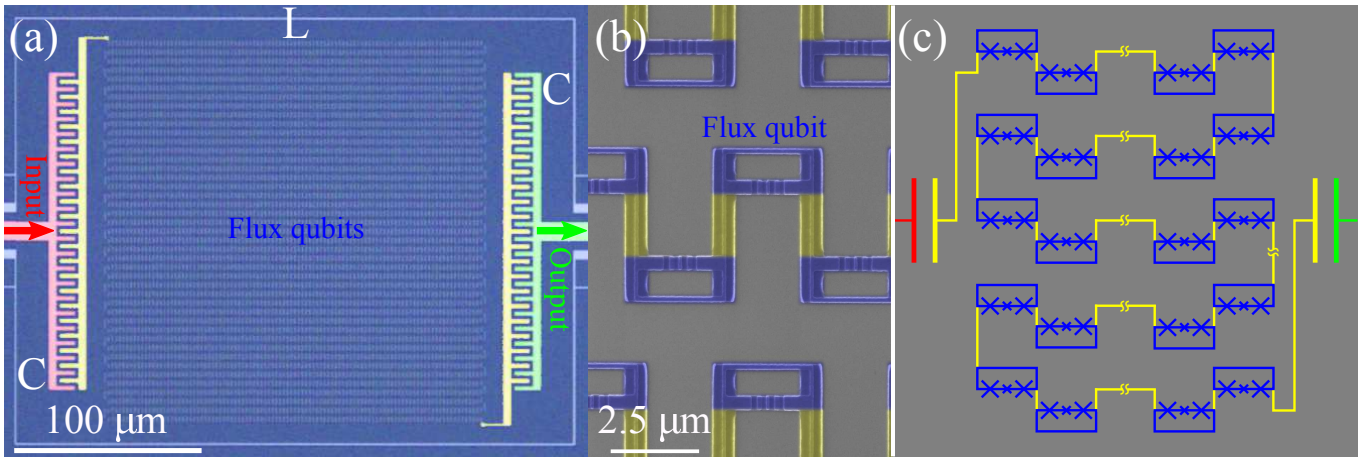

FIG. 1. Our device is composed of 4300 superconducting flux qubits embedded in an LC resonator. These flux qubits are coupled with the resonator via mutual inductance. We show in (a) an optical microscope image, (b) a scanning electron micrograph (in false colors), and (c) a schematic view of our device. Spectroscopy is performed on this device by measuring the photons transmitted from the resonator.

ing flux qubits with a common resonator can overcome this inhomogeneity, because the coupling strength is enhanced by $\sqrt{N}$ times due to the collective effect where N is the number of flux qubits [47, 48]. Actually, we have observed a large energy shift of 250 MHz in the spectroscopy of the resonator. Since the designed coupling strength between a single flux qubit and a resonator is around 16 MHz, such a large dispersive shift indicates a collective enhancement of the coupling strength due to the ensemble of the superconducting flux qubits. We estimate that thousands of superconducting flux qubits contributes to this collective coupling. These results represent the largest number of coupled superconducting qubits realized so far, and this will lead to various applications in quantum information processing.

Experimental results

We fabricate a microwave resonator and 4300 flux qubits on a Si wafer. The flux qubit consists of a loop interrupted by three Al-Al_2O_3-Al Josephson junctions. We designed the area of one junction to be α times smaller than those of the other two junctions. The value of E_J/E_c is 75 in our design where E_J (E_c) denotes a Josephson (charge) energy. The flux qubits share an edge with the inductor line of the resonator.

Our experimental setup is shown in Fig. 1. We measure the microwave transmission properties of the resonator system by a network analyzer. The sample was placed in a dilution refrigerator operating at 20 mK. We can apply magnetic fields perpendicular to the flux qubits, and this can change the operating point of the flux qubit. Also, we can change the temperature from below 10 mK (base temperature) to 230 mK by a heater (See methods section for the details).

Spectroscopy was performed on the resonator coupled with thousands of flux qubits for two separate devices (samples A and B) with different designed α values. By varying the driving microwave frequency and applied magnetic field, the transmitted photon intensity indicates the resonance frequency of our device. In our experiment, we observed a resonator frequency shift due to coupling with the flux qubits. With sample A, we have observed a large negative resonator-frequency shift of $\delta\omega_r/2\pi \simeq 250$ MHz, and the width of the spectrum becomes larger as the frequency shift increases (Fig. 2a.) On the other hand, for sample B, we observed both a negative and a positive frequency shift of tens of MHz (Fig. 2b), and the width of the spectrum becomes broader as the frequency shifts. We also measured the temperature dependence of the resonator frequency for sample B where we plot the frequency of the resonator in the spectroscopic measurements (Fig. 2c). This shows that an increase in the temperature tends to suppress the frequency shift of the resonator due to the thermalization of the flux qubits with small tunneling energies. Moreover, on top of the frequency shift, we observe numerous small energy shifts in the spectroscopy in the experiments (Fig. 2c). These peaks are reproducible over multiple experiments, and so they do not correspond to noise.

Theoretical model

To understand the mechanism causing the frequency shift of the resonator, we model our resonator-qubit ensemble system with a Tavis-Cumming Hamiltonian in the rotat-

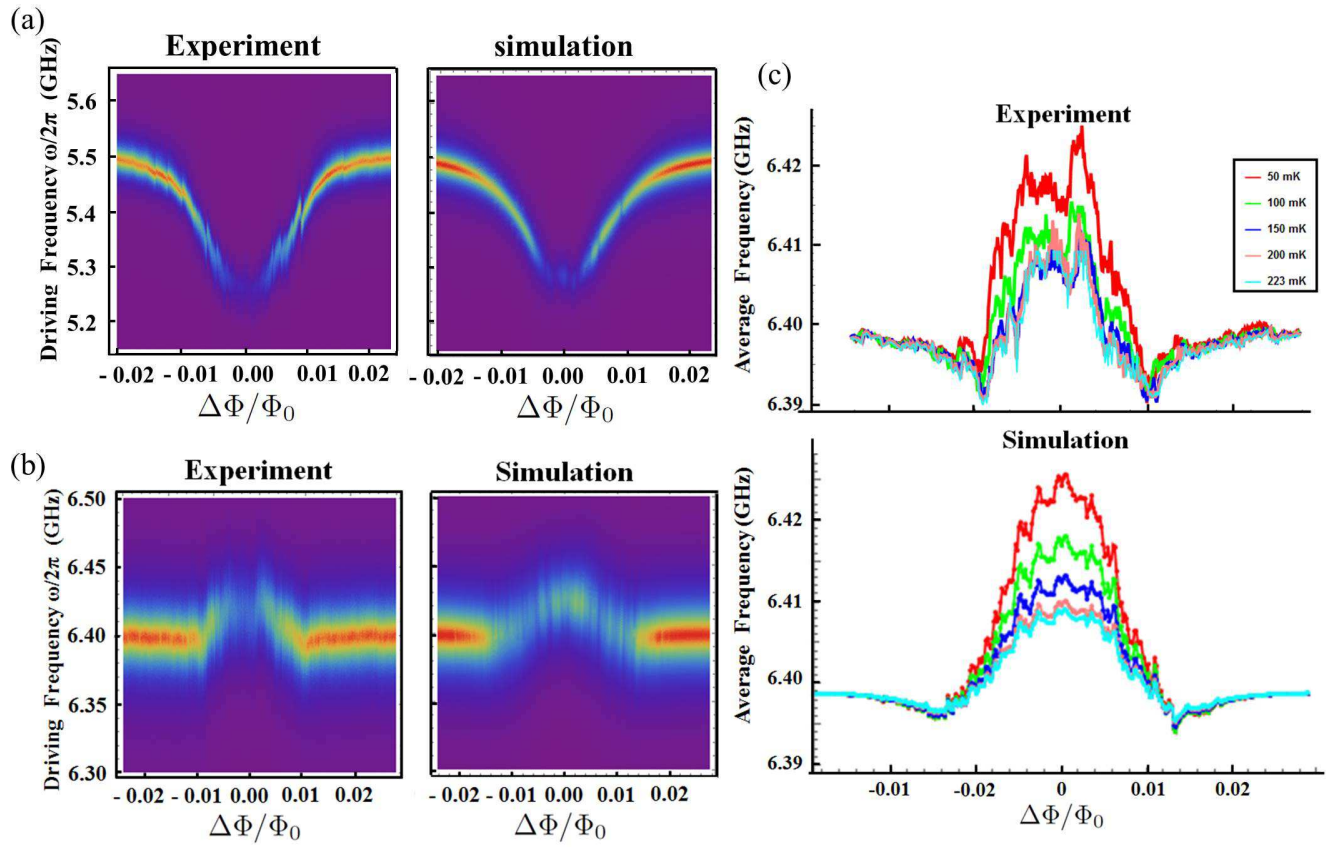

FIG. 2. Experimental results and numerical simulations of the energy spectrum of a microwave resonator coupled to an ensemble of flux qubits. For sample A, we used the parameters $N = 4300$, $\bar{\alpha}$= 0.6285, $\bar{\beta}_1$=$\bar{\beta}_2$=1, $\sigma_S/\bar{\alpha} = \sigma_L^{(1)}/\bar{\beta}^{(1)} = \sigma_L^{(2)}/\bar{\beta}^{(2)} = 0.025$, $\omega_{res}/2\pi = 5.5$ GHz, $\bar{g}'/2\pi$=14.3 MHz, $\delta\epsilon_0'/2\pi$ =2.8 GHz, $\gamma_{qubit}/2\pi$= 50 MHz, and $\gamma_r/2\pi$= 13.3 MHz. For sample B, we used the parameters $N = 4300$, $\bar{\alpha} = 0.7815$, $\bar{\beta}^{(1)} = \bar{\beta}^{(2)}$=1, $\sigma_S/\bar{\alpha} = \sigma_L^{(1)}/\bar{\beta}^{(1)} = \sigma_L^{(2)}/\bar{\beta}^{(2)} = 0.055$, $\omega_{res}/2\pi = 6.4$ GHz, $\bar{g}'/2\pi$=9.2 MHz, $\delta\epsilon_0'/2\pi$ =2.6 GHz, $\gamma_{qubit}/2\pi$= 50 MHz, and $\gamma_r/2\pi$= 12.2 MHz. (c) Temperature dependence of the energy spectrum of a microwave resonator coupled to thousands of flux qubits. We use the same parameters as those in Fig. 2. From the top, we plot the results with T_E=50 mK (red), T_E=100 mK (green), T_E=150 mK (blue), T_E=200 mK (pink), T_E=223 mK (cyan).

ing frame of the microwave driving frequency [49] as

$$H = H_S + H_D + H_I \tag{1}$$

$$H_S = \hbar(\omega_r - \omega)\hat{a}^\dagger\hat{a} + \frac{\hbar}{2}\sum_{j=1}^{N}(\omega_j - \omega)\hat{\sigma}_{z,j} \tag{2}$$

$$H_D = \hbar\lambda(\hat{a}^\dagger + \hat{a}) \tag{3}$$

$$H_I = \hbar\sum_{j=1}^{N} g_j(\hat{\sigma}_j^+\hat{a} + \hat{\sigma}_j^-\hat{a}^\dagger) \tag{4}$$

where $\hat{a}$ ($\hat{a}^\dagger$) represents the annihilation creation operator of the microwave resonator, λ denotes a microwave driving field with a frequency of $\hbar\omega$, $\hbar\omega_r$ denotes the energy of the resonator, $\hbar\omega_j = \sqrt{\Delta_j^2 + \epsilon_j^2}$ denotes the energy of the j th flux qubit where Δ_j is the tunneling energy of the j-th qubit and $\epsilon_j = 2I_j(\Phi_{ex}^{(j)} - \frac{1}{2}\Phi_0)$ is the energy bias. Here, I_j denotes the persistent current of the j-th flux qubit, Φ_0 denotes the flux quantum, $\Phi_{ex}^{(j)}$ denotes the applied magnetic flux. Next, $g_j = \frac{\Delta_j}{\sqrt{\Delta_j^2+\epsilon_j^2}}g_j'$ represents the effective coupling strength where g_j' represents the bare inductive coupling strength calculated from the persistent currents and inductance of the devices, and N denotes the number of flux qubits. We rewrite the energy bias as $\epsilon_j = 2I_j(\Phi_{ex}+\delta\Phi_{ex}^{(j)}-\frac{1}{2}\Phi_0) = 2I_j(\Phi_{ex}-\frac{1}{2}\Phi_0)+\epsilon_{0j}$ where Φ_{ex} denotes the average applied magnetic field and $\epsilon_{0j} = 2I_j\delta\Phi_{ex}^{(j)}$ denotes the energy bias variation caused by the inhomogeneous magnetic flux $\delta\Phi_{ex}^{(j)}$.

We can calculate the transmitted photon intensity of the microwave resonator as follows. By solving the Heisenberg equations with a weak coupling regime when the system is stationary [50–52], we obtain the transmitted photon intensity $T(\omega)$ as follows (See methods section

for the details).

$$|T(\omega)|^2 \simeq \frac{|\lambda|^2}{(\omega-(\omega_{\rm r}+\delta\omega_{\rm r}))^2+(\gamma_{\rm r}+\delta\gamma_{\rm r})^2}$$

$$\delta\omega_{\rm r} = -\sum_{j=1}^{N}\frac{g_j^2(\omega_j-\omega_{\rm r})\cdot\tanh(\frac{\hbar\omega_j}{2k_BT_{\rm E}})}{(\omega_j-\omega_{\rm r})^2+\gamma_j^2} \quad (5)$$

$$\delta\gamma_r = \sum_{j=1}^{N}\frac{g_j^2\gamma_j}{(\omega_j-\omega_{\rm r})^2+\gamma_j^2} \quad (6)$$

$$\gamma_j = (1+(e^{\frac{\hbar\omega_j}{k_BT_{\rm E}}}-1)^{-1})\gamma_{\rm qubit} \quad (7)$$

where $\delta\omega_{\rm r}$ denotes a frequency shift of the resonator and $\delta\gamma_r$ denotes the change in the decay rate of the resonator, $T_{\rm E}$ denotes the temperature of the environment, $\gamma_{\rm r}$ denotes the decay rate of the resonator, and $\gamma_{\rm qubit}$ (γ_j) denotes the energy relaxation rate of the flux qubit at zero (finite) temperature.

The ensemble of flux qubits is affected by inhomogeneous broadening, as it is difficult to make homogeneous junctions, and so the area of each junction has a statistical distribution. This results in variations in the persistent current and the tunneling energy of the flux qubit. The applied magnetic field is also inhomogeneous, which induces the fluctuation distribution in ϵ_0. We assume a Gaussian distribution for the normalized areas of the smaller junction (two larger junctions) with a mean value of $\bar{\alpha}$ ($\bar{\beta}_k$ for $k=1,2$) and a standard deviation of $\sigma_{\rm S}$ ($\sigma_{\rm L}^{(k)}$ for $k=1,2$). It is worth mentioning that g_j' and ϵ_{0j} values are proportional to the I_j value. So we rewrite these as $g_j'=\bar{g}I_j/\bar{I}$ and $\epsilon_{0j}=\epsilon_{0j}'I_j/\bar{I}$ where $\bar{I}$ ($\bar{g}$) denotes the average value of the persistent current (coupling strength), and we assume a Gaussian distribution for the value of ϵ_{0j}' with a mean value of zero and a standard deviation of $\delta\epsilon_0'$. We explain the above in detail in the supplementary materials.

Comparison of experiments and simulations

Dispersive frequency shift. For sample A, we can reproduce the experimental spectroscopic results with our model as shown in the Fig. 2a. From the modeling, the mean value (standard deviation) of the tunneling energy of the flux qubits is estimated as $\bar{\Delta}/2\pi = 9.74$ GHz ($\sigma_\Delta/2\pi = 1.7$ GHz). The negative resonator-frequency shift of $\delta\omega_{\rm res}/2\pi \simeq 250$ MHz can be understood as the dispersive energy shift [6, 53]. Since this experiment is implemented in a dilution refrigerator with a temperature of 50 mK, the flux qubit is prepared in the ground state as long as the qubit energy is much larger than the thermal energy of $k_BT/2\pi\hbar \simeq 1$ GHz. When most of the flux qubit energy is well above the resonator frequency, each qubit induces a negative resonator frequency shift of $-\frac{|g_j|^2}{\omega_j-\omega_{\rm r}}$. Due to a collective effect, we can achieve a large dispersive shift of $\delta\omega_{\rm res}/2\pi \simeq 250$ MHz for sample A. Although the individual coupling $\overline{g}'/2\pi(=14.3$MHz) is small, the collective effect enhances the coupling strength $\sqrt{N}$ times [47, 48]. Also, the resonator width tends to becomes larger as the flux qubits approaches the degeneracy point for $\epsilon \simeq 0$ (see Fig. 2a.) This is reasonable because the detuning between the flux qubit and the resonator becomes smaller as the operating point of the flux qubits approaches to the degeneracy, and this should induce additional decay in the resonator.

Importantly, these experimental results provide an order estimation of the number of flux qubits coupled with the resonator. The bare coupling strength between a single flux qubit and the resonator is described as $g_j' = M_{\rm qr}I_j\sqrt{\frac{\omega_{\rm r}}{2\hbar L}}$ where L denotes the inductance of the resonator and $M_{\rm qr}$ denotes a mutual inductance between the flux qubit and the resonator. We can estimate these values as $M \simeq 10$ pH and $L \simeq 100$ nH from numerical simulations, and so we obtain $g_j'/2\pi \simeq 16$ MHz for $\omega_{\rm r}/2\pi = 5.5$ GHz and $I_j = 250$ nA. On the other hand, by reproducing the spectroscopic measurements in Fig. 2, we estimate the average bare coupling strength as $\overline{g}'/2\pi \simeq 14.3$ MHz where we assume $N = 4300$. This small discrepancy in the estimated coupling strength of g_j' might indicate that, although we intended to fabricate 4300 flux qubits, some of them would not work as qubits because of imperfect fabrication. This could mean that the actual number of flux qubits contributing to the collective enhancement might be smaller than 4300. However, from these estimations, we can at least conclude that thousands of flux qubits should be involved in the collective coupling with the resonator, because otherwise experimental results such as the large dispersive shift of $\delta\omega_{\rm res}/2\pi \simeq 250$ MHz cannot be explained by the parameters $N < 1000$ and $g_j'/2\pi \simeq 16$ MHz.

Thermal effects on the energy shift. For sample B, we can reproduce the experimental spectroscopic results with our theoretical model as shown in Fig. 2b. From these theoretical calculations, the mean value (standard deviation) of the tunneling energy of the flux qubits is estimated to be $\bar{\Delta}/2\pi = 1.17$ GHz ($\sigma_\Delta/2\pi = 1.1$ GHz). Both negative and positive frequency shifts of the resonator can occur when the tunneling energy of the flux qubit is smaller than the resonator frequency. In this case, the flux-qubit energy can cross the resonator frequency by applying a magnetic field. Unfortunately, due to a large inhomogeneous broadening of a few GHz, we cannot observe the vacuum Rabi splitting of the qubit-resonator anticrossing. However, the positive and negative energy shifts indicate the existence of coupling between the flux-qubit ensemble and the resonator. Interestingly, the dispersive shift around the degeneracy point for sample B is $\delta\omega_{\rm res}/2\pi \simeq 16$ MHz, which is much smaller than the shift observed in sample A. This is due to the small tunneling energy ($\bar{\Delta}/2\pi \sim 1$ GHz) of the flux qubit where the thermal energy depolarizes the flux qubit, which weakens the dispersive shift.

We can reproduce the temperature dependence of the spectroscopic measurements with our model as shown in

Fig. 2c. The temperature dependence becomes clearer as the flux qubit approaches the degeneracy point. Since the energy of the flux qubit reaches its minimum at the degeneracy point, the state of the flux qubit strongly depends on the environmental temperature because of the small tunneling energy, and this induces a temperature dependent dispersive shift. On the other hand, far from the degeneracy point, the resonator frequency shift becomes almost independent of the temperature, because the flux qubit is not significantly affected by the thermal effect caused by the large flux qubit energy.

Discrete nature of the qubits. Interestingly, on top of the dispersive shift, we observe numerous small energy shifts in the spectroscopy in the experiments and simulations (see Fig. 2c). This is because a large finite number of flux qubits are coupled with the resonator. If a single qubit was coupled with the resonator, only the dispersive shift and/or the vacuum Rabi splitting should be observed in the spectroscopy because of the change of the eigenenergy of the resonator coupled with a qubit [6, 53]. On the other hand, in the limit of a large number of qubits coupled with the resonator, we should also observe the dispersive frequency shift and/or vacuum Rabi splitting in the spectroscopy, because we can consider the qubit ensemble to be a single harmonic oscillator as a consequence of the continuum limit [52]. In the experiments described here, since the resonator is coupled with thousands of qubits, which is large but finite number, we observe numerous additional energy shifts in the spectroscopy due to the discrete nature of each flux qubit.

Discussion

In conclusion, we have reported experiments that show collective coupling between a superconducting resonator and an ensemble of superconducting flux qubits. We have observed the large dispersive frequency shift of the resonator, and this demonstrates a collective behavior of the superconducting flux qubits. A quantitative analysis indicates that thousands of superconducting flux qubits contribute to the collective coupling. These results represent the largest number of coupled superconducting qubits realized so far. Our system has many potential applications including quantum metamaterials, quantum metrology, and a quantum simulator.

Methods

Experimental setup.

We fabricate a microwave resonator and 4300 flux qubits on a Si wafer by using electron beam lithography and conventional angled evaporation technique. Here, the Si wafer has SiO_2 thin film. Our flux qubit has three Al-Al_2O_3-Al Josephson junctions.

Our experimental setup is described in the Fig. 3. We measure the microwave transmission properties of the resonator system around 6 GHz by a network analyzer. To amplify the output microwave signal, we prepare HEMT amplifier on 4K stage. We insert attenuators on each temperature stage. Also, we insert band pass filters and isolators to avoid thermal noise coming from room temperature and amplifier. We can apply magnetic fields perpendicular to qubits to change the operating points of the superconducting flux qubits.

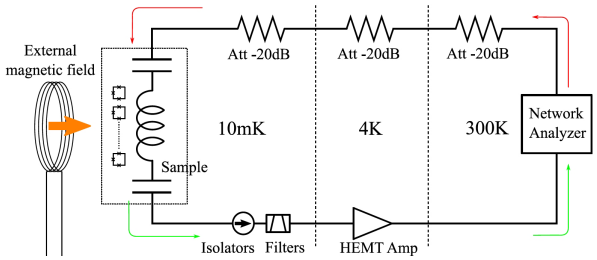

FIG. 3. Schematic of our experiment setup. Here, we measure the microwave transmission properties of the resonator with a network analyzer. The microwave resonator is inductively coupled with 4500 flux qubits.

We can change the temperature from 10 mK to 230 mK. To measure the temperature, we can use a RuO_2 thermometer at a mixing chamber, and we stabilize it by using a PID feedback controlled heater.

Theoretical model. We describe the theoretical model that we used for the results described in the main text.

Firstly, we derive a formula for the transmitted photon intensity when the effect of the thermal energy is negligible. If the excited state of the flux qubit is not significantly populated with weak microwave driving, we can approximate the flux qubit as a harmonic oscillator [54]. Here, only the lowest two levels of the harmonic oscillator are occupied, and the effect of the other levels is negligible due to the weak driving power. With the replacement of $\hat{\sigma}_j^+ \rightarrow \hat{b}_j^\dagger$, we can represent Heisenberg equations based on the Hamiltonian in Eq. 1

$$i\hbar\frac{d\hat{a}}{dt} = \hbar\lambda + \hbar(\omega_r - \omega - i\gamma_r)\hat{a} + \sum_j \hbar g_j \hat{b}_j,$$

$$i\hbar\frac{d\hat{b}_j}{dt} = \hbar(\omega_j - \omega - i\gamma_{\rm qubit})\hat{b}_j + \hbar g_j \hat{a}$$

We use a steady condition such as $\frac{d\hat{a}}{dt} = 0$ and $\frac{d\hat{b}_j}{dt} = 0$ and we obtain

$$\hat{a} = \frac{\lambda}{\omega - \omega_r + i\gamma_r - \sum_j \frac{g_j^2}{\omega - \omega_j + i\gamma_{\rm qubit}}}. \quad (8)$$

In a weak coupling regime, we can assume $|\omega - \omega_r| \ll$

$|\omega_{\rm r}-\omega_j+i\gamma_j|$ for $j=1,2,\cdots,N$, and so we obtain

$$\begin{aligned}\hat{a} &\simeq \frac{\lambda}{(\omega-(\omega_{\rm r}+\delta\omega_{\rm r}))+i(\gamma_{\rm r}+\delta\gamma_{\rm r})}\\ \delta\omega_{\rm r} &= -\sum_j g_j^2\frac{\omega_j-\omega_{\rm r}}{(\omega_j-\omega_{\rm r})^2+\gamma_{\rm qubit}^2}\\ \delta\gamma_{qubit} &= \sum_j g_j^2\frac{\gamma_{\rm qubit}}{(\omega_j-\omega_{\rm r})^2+\gamma_{\rm qubit}^2}\end{aligned} \tag{9}$$

Secondly, we derive a formula for the resonator frequency shift induced by the detuned flux qubits whose energies are comparable to the thermal energy. Due to the energy difference between the microwave resonator and the flux qubits, we can use a dispersive Hamiltonian to describe this system as

$$\begin{aligned}H_{\rm disp} &\simeq \hbar\sum_j(\frac{\omega_j-\omega}{2}+\frac{g_j^2}{2(\omega_j-\omega_{\rm r})})\hat{\sigma}_{z,j}\\ &+\hbar(\omega_{\rm r}-\omega+\sum_j g_j^2\frac{\hat{\sigma}_{z,j}}{\omega_j-\omega_{\rm r}})\hat{a}^\dagger\hat{a}+\hbar\lambda(\hat{a}+\hat{a}^\dagger)\end{aligned} \tag{10}$$

In this case, we have a dispersive shift for the energy of the microwave resonator such as

$$\delta\omega_{\rm r}=\sum_j g_j^2\frac{\langle\sigma_{z,j}\rangle}{\omega_j-\omega_{\rm r}} \tag{11}$$

where $\langle\hat{\sigma}_{z,j}\rangle$ denotes the expectation value of $\hat{\sigma}_{z,j}$. Since the flux qubit is in a thermal equilibrium, we obtain

$$\delta\omega_{\rm r}=-\sum_j g_j^2\frac{\tanh(\frac{\hbar\omega_j}{2k_BT_{\rm E}})}{\omega_j-\omega_{\rm r}} \tag{12}$$

Also, since the energy relaxation rate of a qubit with an energy of ω_j is proportional to $(1+\overline{N})$ where $\overline{N}=(e^{\frac{\hbar\omega_j}{k_BT_{\rm E}}}-1)^{-1}$ denotes the Bose-Einstein occupation number of the environmental bosonic modes [50], we assume

$$\gamma_j=(1+(e^{\frac{\hbar\omega_j}{k_BT_{\rm E}}}-1)^{-1})\gamma_{\rm qubit} \tag{13}$$

and so we can take the thermal effect into account in the decay rate of the flux qubit.

Therefore, from the equations described above, we derive the following phenomenological function

$$\langle\hat{a}^\dagger\hat{a}\rangle\simeq\frac{\lambda^2}{(\omega-(\omega_{\rm r}+\delta\omega_{\rm r}))^2+(\gamma_{\rm r}+\delta\gamma_{\rm r})^2} \tag{14}$$

where we have

$$\delta\omega_{\rm r}=-\sum_j g_j^2\frac{\tanh(\frac{\hbar\omega_j}{2k_BT_{\rm E}})(\omega_j-\omega_{\rm r})}{(\omega_j-\omega_{\rm r})^2+\gamma_j^2} \tag{15}$$

$$\delta\gamma_{qubit}=\sum_j g_j^2\frac{\gamma_j}{(\omega_j-\omega_{\rm r})^2+\gamma_j^2}. \tag{16}$$

This function will coincide with Eq. (8) or (12) in the limit of a low temperature or a large detuning. Since the number of photons inside the resonator corresponds to the intensity of the transmitted photons [52], we can use this function to reproduce the experimental results. It is worth mentioning that we observed experimentally the applied magnetic flux dependence of the microwave driving amplitude $\lambda=\lambda(\Phi_{\rm ex})$. Although this cannot be explained by our theoretical model, we obtain the shape of $\lambda(\Phi_{\rm ex})$ from the experiment, and substitute this into our theoretical model to reproduce the spectroscopic measurements (See the supplementary materials for details).

Acknowledgments

We thank S. Endo, I. Natsuko, and N. Lambert for their useful comments. This work was supported by JSPS KAKENHI Grant 15K17732, JSPS KAKENHI Grant No.25220601, the Commissioned Research No. 158 of NICT, and MEXT KAKENHI Grant Number 15H05870.

Author contributions

All authors contributed extensively to the work presented in this paper. K. K fabricated the device and carried out measurements. Y.M., C.D., and W.J.M provided theoretical support and analysis. Y.M. wrote the manuscript, with feedback from all authors. H.Y., W.J.M. and S.S. supervised the project.

SUPPLEMENTARY FIGURES

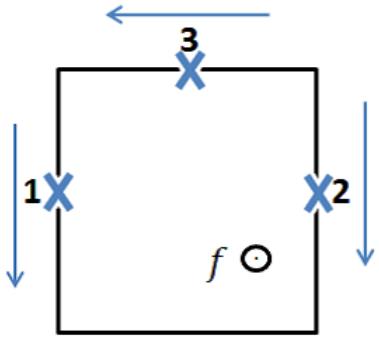

FIG. 4. Schematic of a superconducting flux qubit with three Josephson junctions. The area of one junction is designed to be α times smaller than those of the other two junctions.

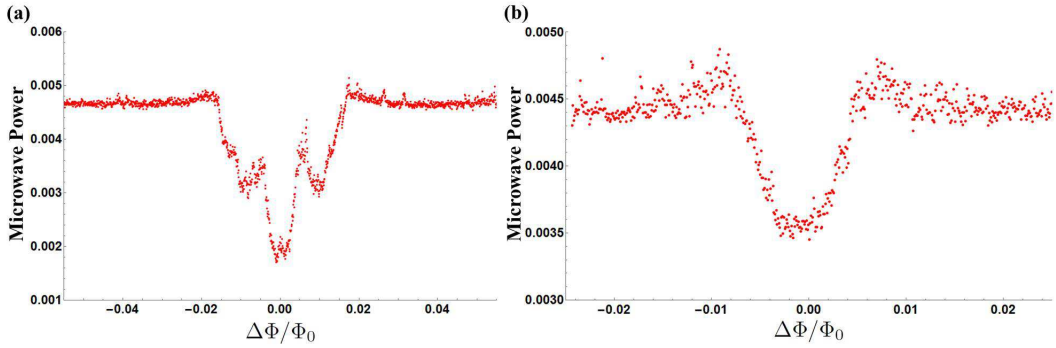

FIG. 5. Applied magnetic flux dependence of the microwave amplitude in our experiment. For a fixed amount of applied magnetic flux, we fit the experimental spectroscopic results (shown in Fig. 2 in the main text) by using $f(\omega) = \frac{\Lambda^2}{(\omega-\omega_{\rm av}+\gamma^2)}$ and obtain the fitting parameters of Λ, $\omega_{\rm av}$, and γ. We plot Λ here for sample A (left) and sample B (right). These plots show that the microwave driving amplitude is dependent on the applied magnetic flux.

SUPPLEMENTARY NOTE 1: INHOMOGENEITY OF JOSEPHSON JUNCTIONS

We describe how we take the inhomogeneity of the Josephson Junctions into account in our model. We consider a superconducting circuit with three Josephson junctions as shown in the Fig. 4 The Lagrangian of this system [46] can be written as

$$L = T - U \tag{17}$$

$$U = \sum_{j=1}^{3} (\frac{\Phi_0}{2\pi} I_{\rm C}^j (1 - \cos(\phi_j)) \tag{18}$$

$$T = \sum_{j=1}^{3} \frac{1}{2} C_j (\frac{\Phi_0}{2\pi})^2 \dot{\phi_j}^2 \tag{19}$$

where U denotes the total potential energy, T denotes the total kinetic energy, ϕ_j $(j = 1, 2, 3)$ denotes the phase difference between the junctions, C_j denotes the capacitance of the Josephson junction, $I_{\rm C}^j$ denotes the critical current, $\Phi_{\rm ext}$ denotes the flux due to the external magnetic field, and $\Phi_0 = \frac{\hbar}{2e}$ denotes the magnetic flux quantum. $E_J^{(j)} = \frac{\Phi_0}{2\pi} I_{\rm C}^j$ denotes the characteristic scale of the Josephson energy while $E_c = \frac{e^2}{2C_j}$ sets the characteristic electric energy. We have a condition $\phi_1 - \phi_2 + \phi_3 = 2\pi f$ with $f = \frac{\Phi \rm ext}{\Phi_0}$. It is worth mentioning that C_j and $I_{\rm C}^j$ are proportional to the size of the junction. The area for one junction is α times smaller than those for the other two junctions if the device is fabricated as designed. However, Josephson junctions are very sensitive to experimental conditions, and the size of the junctions becomes inhomogeneous. To consider this inhomogeneity, we assume a Gaussian distribution for normalized areas of the smaller junction (two larger junctions) with a mean value of $\bar{\alpha}$ ($\bar{\beta}_k$ for $k = 1, 2$) and a standard deviation of $\sigma_{\rm S}$ ($\sigma_{\rm L}^{(k)}$ for $k = 1, 2$). By solving this, we can calculate the energies of the ground state and excited state for a given external magnetic flux, which provides us with the values of the tunneling energy Δ_j and the persistent current I_j of the flux qubit [46].

SUPPLEMENTARY NOTE 3: APPLIED MAGNETIC FLUX DEPENDENCE OF MICROWAVE DRIVING AMPLITUDE

In the spectroscopic measurements shown in Fig. 2 in the main text, we experimentally observe a Lorentz distribution for a fixed amount of applied magnetic flux. We fit the spectrum by a function of $f(\omega) = \frac{\Lambda^2}{(\omega-\omega_{\rm av}+\gamma^2)}$, and obtain the fitting parameters of $\omega_{\rm av}$, γ, and Λ. Our theoretical model described in the main text predicts that the microwave amplitude will be independent of the applied magnetic flux. However, the Λ value obtained from the fitting has some dependence on the applied magnetic flux as shown in Fig. (5). Although this cannot be explained by our theoretical model, we substitute this into our theoretical model ($\lambda = \Lambda$) to reproduce the spectroscopic measurements.

A possible reason is that the properties of the flux qubit change due to the applied magnetic field, and this may also change the impedance of the resonator. Such variations in the impedance induce additional reflection of the input photon, and this could explain the dependence of the driving strength on the applied magnetic fields.

* kakuyanagi.kosuke@lab.ntt.co.jp

[1] Dowling, J. P. & Milburn, G. J. Quantum technology: the second quantum revolution. *Philosophical Transactions of the Royal Society of London A: Mathematical, Physical and Engineering Sciences* **361**, 1655–1674 (2003).

[2] Ladd, T. D. *et al.* Quantum computers. *Nature* **464**, 45–53 (2010).

[3] Xiang, Z.-L., Ashhab, S., You, J. & Nori, F. Hybrid quantum circuits: Superconducting circuits interacting with other quantum systems. *Reviews of Modern Physics* **85**, 623 (2013).

[4] Benjamin, S. C., Lovett, B. W. & Smith, J. M. Prospects for measurement-based quantum computing with solid state spins. *Laser & Photonics Reviews* **3**, 556–574 (2009).

[5] Paz, J. P. Quantum engineering: protecting the quantum world. *Nature* **412**, 869–870 (2001).

[6] Blais, A. *et al.* Quantum-information processing with circuit quantum electrodynamics. *Phys. Rev. A* **75**, 032329 (2007).

[7] Tsomokos, D. I., Ashhab, S. & Nori, F. Fully connected network of superconducting qubits in a cavity. *New Journal of Physics* **10**, 113020 (2008).

[8] Schmidt, S. & Koch, J. Circuit qed lattices: towards quantum simulation with superconducting circuits. *Annalen der Physik* **525**, 395–412 (2013).

[9] Georgescu, I., Ashhab, S. & Nori, F. Quantum simulation. *Reviews of Modern Physics* **86**, 153 (2014).

[10] Hepp, K. & Lieb, E. H. On the superradiant phase transition for molecules in a quantized radiation field: The dicke maser model. *Annals of Physics* **76**, 360–404 (1973).

[11] Wang, Y. K. & Hioe, F. Phase transition in the dicke model of superradiance. *Phys. Rev. A* **7**, 831 (1973).

[12] Emary, C. & Brandes, T. Chaos and the quantum phase transition in the dicke model. *Phys. Rev. E* **67**, 066203 (2003).

[13] Lambert, N., Chen, Y.-n., Johansson, R. & Nori, F. Quantum chaos and critical behavior on a chip. *Phys. Rev. B* **80**, 165308 (2009).

[14] Lambert, N., Emary, C. & Brandes, T. Entanglement and the phase transition in single-mode superradiance. *Phys. Rev. Lett.* **92**, 073602 (2004).

[15] Zou, L. *et al.* Implementation of the dicke lattice model in hybrid quantum system arrays. *Phys. Rev. Lett.* **113**, 023603 (2014).

[16] Kitagawa, M. & Ueda, M. Squeezed spin states. *Phys. Rev. A* **47**, 5138 (1993).

[17] Bennett, S. *et al.* Phonon-induced spin-spin interactions in diamond nanostructures: application to spin squeezing. *Phys. Rev. Lett.* **110**, 156402 (2013).

[18] Tanaka, T. *et al.* Proposed robust entanglement-based magnetic field sensor beyond the standard quantum limit. *Phys. Rev. Lett.* **115**, 170801 (2015).

[19] Zheludev, N. I. The road ahead for metamaterials. *Science* **328**, 582–583 (2010).

[20] Soukoulis, C. M. & Wegener, M. Past achievements and future challenges in the development of three-dimensional photonic metamaterials. *Nature Photonics* **5**, 523–530 (2011).

[21] Zheludev, N. I. & Kivshar, Y. S. From metamaterials to metadevices. *Nature Materials* **11**, 917–924 (2012).

[22] Ricci, M., Orloff, N. & Anlagea, S. M. Superconducting metamaterials. *Appl. Phys. Lett.* **87**, 034102 (2005).

[23] Lazarides, N. & Tsironis, G. Rf superconducting quantum interference device metamaterials. *Appl. Phys. Lett.* **90**, 163501 (2007).

[24] Anlage, S. M. The physics and applications of superconducting metamaterials. *Journal of Optics* **13**, 024001 (2011).

[25] Jung, P., Butz, S., Shitov, S. V. & Ustinov, A. V. Low-loss tunable metamaterials using superconducting circuits with josephson junctions. *Appl. Phys. Lett.* **102**, 062601 (2013).

[26] Zhu, X. *et al.* Coherent coupling of a superconducting flux qubit to an electron spin ensemble in diamond. *Nature* **478**, 221–224 (2011).

[27] Saito, S. *et al.* Towards realizing a quantum memory for a superconducting qubit: Storage and retrieval of quantum states. *Phys. Rev. Lett.* **111**, 107008 (2013).

[28] Kubo, Y. *et al.* Hybrid quantum circuit with a superconducting qubit coupled to a spin ensemble. *Phys. Rev. Lett.* **107**, 220501 (2011).

[29] Zhu, X. *et al.* Observation of dark states in a superconductor diamond quantum hybrid system. *Nature Communications* **3424**, 4524 (2014).

[30] Matsuzaki, Y. *et al.* Improving the lifetime of the nitrogen-vacancy-center ensemble coupled with a superconducting flux qubit by applying magnetic fields. *Phys. Rev. A* **91**, 042329 (2015).

[31] Putz, S. *et al.* Protecting a spin ensemble against decoherence in the strong-coupling regime of cavity qed. *Nature Physics* **10**, 720–724 (2014).

[32] Tabuchi, Y. *et al.* Coherent coupling between a ferromagnetic magnon and a superconducting qubit. *Science* **349**, 405–408 (2015).

[33] Bienfait, A. *et al.* Reaching the quantum limit of sensitivity in electron spin resonance. *Nature nanotechnology* (2015).

[34] Clarke, J. & Wilhelm, F. Superconducting quantum bits. *Nature* **453**, 1031 (2007).

[35] Makhlin, Y., Schön, G. & Shnirman, A. Quantum-state engineering with josephson-junction devices. *Reviews of modern physics* **73**, 357 (2001).

[36] Paauw, F., Fedorov, A., Harmans, C. M. & Mooij, J. Tuning the gap of a superconducting flux qubit. *Phys. Rev. Lett.* **102**, 090501 (2009).

[37] Zhu, X., Kemp, A., Saito, S. & Semba, K. Coherent operation of a gap-tunable flux qubit. *Applied Physics Letters* **97**, 102503–102503 (2010).

[38] Reed, M. *et al.* Fast reset and suppressing spontaneous emission of a superconducting qubit. *Applied Physics Letters* **96**, 203110 (2010).

[39] Niskanen, A. *et al.* Quantum coherent tunable coupling of superconducting qubits. *Science* **316**, 723–726 (2007).

[40] Harrabi, K., Yoshihara, F., Niskanen, A., Nakamura, Y. & Tsai, J. Engineered selection rules for tunable coupling in a superconducting quantum circuit. *Phys. Rev. B* **79**, 020507 (2009).

[41] Inomata, K. *et al.* Microwave down-conversion with an impedance-matched λ system in driven circuit qed. *Phys. Rev. Lett.* **113**, 063604 (2014).

[42] Fink, J. *et al.* Dressed collective qubit states and the tavis-cummings model in circuit qed. *Phys. Rev. Lett.* **103**, 083601 (2009).

[43] Mlynek, J. A. *et al.* Demonstrating w-type entanglement of dicke states in resonant cavity quantum electrodynamics. *Phys. Rev. A* **86**, 053838 (2012).

[44] Feng, M. *et al.* Exploring the quantum critical behaviour in a driven tavis-cummings circuit. *Nature Communications* **6** (2015).

[45] Macha, P. & *et al.* Implementation of a quantum metamaterial using superconducting qubits. *Nature Commu-*

nications **5** (2014).

[46] Orlando, T. *et al.* Superconducting persistent-current qubit. *Phys. Rev. B* **60**, 15398 (1999).

[47] Imamoğlu, A. Cavity qed based on collective magnetic dipole coupling: spin ensembles as hybrid two-level systems. *Phys. Rev. Lett.* **102**, 083602 (2009).

[48] Wesenberg, J. *et al.* Quantum computing with an electron spin ensemble. *Phys. Rev. Lett.* **103**, 70502 (2009).

[49] Tavis, M. & Cummings, F. W. Exact solution for an n-molecule?radiation-field hamiltonian. *Physical Review* **170**, 379 (1968).

[50] Gardiner, C. W. & Zoller, P. *Quantum Noise* (Springer, Berlin, 2004).

[51] Collett, M. & Gardiner, C. Squeezing of intracavity and traveling-wave light fields produced in parametric amplification. *Phys. Rev. A* **30**, 1386–1391 (1984).

[52] Diniz, I. *et al.* Strongly coupling a cavity to inhomogeneous ensembles of emitters: Potential for long-lived solid-state quantum memories. *Phys. Rev. A* **84**, 063810 (2011).

[53] Wallraff, A. *et al.* Strong coupling of a single photon to a superconducting qubit using circuit quantum electrodynamics. *Nature* **431**, 162–167 (2004).

[54] Houdré, R., Stanley, R. & Ilegems, M. Vacuum-field rabi splitting in the presence of inhomogeneous broadening: Resolution of a homogeneous linewidth in an inhomogeneously broadened system. *Phys. Rev. A* **53**, 2711 (1996).